European Radiology (2019) 29:2837–2847
https://doi.org/10.1007/s00330-018-5789-0

COMPUTED TOMOGRAPHY

Dual-layer dual-energy computed tomography for the assessment of hypovascular hepatic metastases: impact of closing k-edge on image quality and lesion detectability

Yasunori Nagayama[1] · Ayumi Iyama[1] · Seitaro Oda[1] · Narumi Taguchi[1] · Takeshi Nakaura[1] · Daisuke Utsunomiya[1] · Yoko Kikuchi[1] · Yasuyuki Yamashita[1]

Received: 30 June 2018 / Revised: 17 August 2018 / Accepted: 21 September 2018 / Published online: 30 October 2018

Abstract

Objectives To evaluate the image quality of virtual-monoenergetic-imaging (VMI) from dual-layer dual-energy CT (DLCT) for the assessment of hypovascular liver metastases and its effect on lesion detectability.

Methods Eighty-one patients with hypovascular-liver-metastases undergoing portal-venous-phase abdominal DLCT were included. Polyenergetic-images (PEI) and VMI at 40–200 keV ($VMI_{40–200}$, 10-keV interval) were reconstructed. Image noise, tumor-to-liver contrast, and contrast-to-noise ratio (CNR) of hepatic parenchyma and metastatic nodules ($n = 288$) were measured to determine the optimal monoenergetic levels. Two radiologists independently and subjectively assessed the image quality (image contrast, image noise, and diagnostic confidence) of PEI and optimal VMI on 5-point scales to determine the best energy. For 38 patients having up to 10 metastases each with diameters < 25 mm (153 lesions), we compared blindly assessed lesion detectability and conspicuity between PEI and VMI at the best energy.

Results Image noise of $VMI_{40–200}$ was consistently lower than that of PEI ($p < 0.01$). Tumor-to-liver contrast and CNR increased as the energy decreased with CNR at $VMI_{40–70}$ being higher than that observed on PEI ($p < 0.01$). The highest subjective score for diagnostic confidence was assigned at VMI_{40} followed by $VMI_{50–70}$, all of which were significantly better than that of PEI ($p < 0.01$, kappa = 0.75). Lesion detectability at VMI_{40} was significantly superior to PEI, especially for lesions with diameters of < 10 mm ($p < 0.01$, kappa ≥ 0.6).

Conclusions $VMI_{40–70}$ provided a better subjective and objective image quality for the evaluation of hypovascular liver metastases, and the lesion detectability was improved with use of VMI_{40} compared with conventional PEI.

Key Points

- *DLCT-VMI at 40–70 keV provides a superior subjective and objective image quality compared with conventional PEI for the assessment of hypovascular hepatic metastases during portal venous phase.*
- *Tumor-to-liver contrast and CNR of hypovascular hepatic metastases was maximized at 40 keV without a relevant increase in the image noise.*
- *VMI at 40 keV yields a superior lesion detectability, especially for small (< 1 cm) metastatic nodules compared with conventional PEI.*

Keywords Multidetector computed tomography · Dual-energy scanned projection radiography · Metastasis · Image enhancement

Abbreviations

CNR	Contrast-to-noise ratio
$CTDI_{vol}$	Volume CT dose index
DECT	Dual-energy CT
DLCT	Dual-layer dual-energy CT
PEI	Polyenergetic image
ROI	Region of interest
SSDE	Size-specific dose estimate
VMI	Virtual monoenergetic imaging

✉ Yasunori Nagayama
y.nagayama1980@gmail.com

[1] Department of Diagnostic Radiology, Graduate School of Medical Sciences, Kumamoto University, 1-1-1, Honjo, Chuo-ku, Kumamoto 860-8556, Japan

Introduction

One of the major roles of abdominal imaging in patients with cancer is the detection of hypovascular hepatic metastases. Contrast-enhanced computed tomography (CT) is widely accepted as the primary imaging modality for preoperative staging and post-treatment surveillance, but it is less sensitive for detecting small hepatic metastases compared with magnetic resonance imaging (MRI) [1, 2]. The identification of small hypoattenuating hepatic lesions can be improved by increasing the tumor-to-liver contrast [3] but becomes challenging when the image noise increases [4, 5]. In this context, various techniques, such as optimization of contrast medium injection [6, 7], lowering the tube voltage [8], and iterative reconstruction algorithms [9, 10], have been developed and utilized to improve the lesion contrast or reduce the image noise.

Virtual-monoenergetic-imaging (VMI) derived from dual-energy CT (DECT) can also be used to enhance the depiction of hepatic tumors. VMI mimics the image that would be obtained from single-photon energy. VMI at lower monoenergetic levels theoretically yields a better depiction of hepatic lesions that show hyper- and hypovascularity, relative to surrounding hepatic parenchyma because iodine attenuation is steeply increased as the monoenergetic level approaches the iodine K-edge (33.2 keV). Previous studies on tube-based DECT have shown that hypervascular hepatic lesions during arterial phase are better depicted at lower-keV VMI [11–13]. However, few investigations have sought to determine whether the lower keV images can improve the depiction of hypovascular metastases during the portal-venous-phase, especially for small lesions that are more susceptible to increased noise observed at lower monoenergetic levels. Some authors who investigated the usefulness of tube-based DECT for the assessment of hypovascular hepatic lesions have demonstrated that substantial increase in image noise has restricted the diagnostic usability of the VMI at the lowest energy range, such as 40 keV, despite the highest image contrast [14–16].

Among currently available DECT approaches, dual-layer dual-energy CT (DLCT) has been recently introduced as a first detector-based DECT solution. DLCT measures fully matched dual-energy data across two layers of detectors. This design allows for basis decomposition in the projection domain without need for angular and temporal interpolation. This enables noise variation reduction across all energies by accounting for the anti-correlated noise in the reconstruction process [17–19]. Additionally, DLCT provides opportunities to directly compare the image quality and diagnostic performance between VMI and true conventional polyenergetic image (PEI). Recent studies on abdominal DLCT have demonstrated that the image quality and delineation of hyperenhancing intraabdominal pathologies can be improved with the use of lower-keV VMI compared with PEI owing to an improved iodine contrast without increasing the image noise [17, 20, 21]. However, to our knowledge, the clinical benefits of DLCT-VMI for the evaluation of hypovascular hepatic metastases have not yet been determined. Given the inherent differences in imaging performance between different DECT systems [18, 19], the results obtained with tube-based DECT scanners could not be directly transposable to the novel DLCT system; thus, it may be relevant and valuable to investigate the diagnostic usability of DLCT-VMI for this clinically important and frequent diagnostic task.

In this study, we aimed to evaluate the image quality and potential added value of VMI derived from DCLT, in comparison with conventional PEI, for the detection of hypovascular hepatic metastases during the portal venous phase.

Materials and methods

This retrospective study received institutional review board approval; the requirement for written informed consent was waived. Figure 1 presents the study flowchart.

Patients

We identified consecutive 95 adults diagnosed with hepatic metastases who underwent portal venous phase abdominal imaging with a DLCT scanner (IQon spectral CT; Philips healthcare) between January 2017 and December 2017. We excluded 12 patients, who received a reduced contrast medium protocol owing to renal dysfunction, and two patients with hyperattenuating metastases. Accordingly, 81 patients (38 males and 43 females; age, 63.3 ± 11.7 years; body mass index [BMI], 21.7 ± 3.2 kg/m^2) with 923 hypovascular hepatic metastases (1–80 lesions per patient) were included in this study. In this cohort, the primary cancer sites were colorectal ($n = 22$), breast ($n = 13$), stomach ($n = 12$), pancreas ($n = 8$), lung ($n = 6$), esophagus ($n = 5$), bile duct or gallbladder ($n = 4$), kidney ($n = 3$), skin ($n = 3$), small intestine ($n = 2$), ovary ($n = 1$), duodenum ($n = 1$), and pharynx ($n = 1$). The confirmative diagnosis of hepatic metastases was made by the consensus of two board-certified radiologists with 10 and 21 years of experience in abdominal CT, respectively. All lesions were either newly developed, compared with previous imaging studies, or increased or decreased in size after chemotherapy compared with previous or subsequent CT examinations [8, 14]. In this study, hypovascular hepatic lesion was defined as the lesion showing hypoattenuation relative to surrounding hepatic parenchyma at portal-venous-phase CT images.

Imaging protocol

Scanning was performed with the following parameters: tube voltage, 120 kVp; tube current, 78–179 mAs (automated exposure control); helical pitch, 0.798; detector collimation,

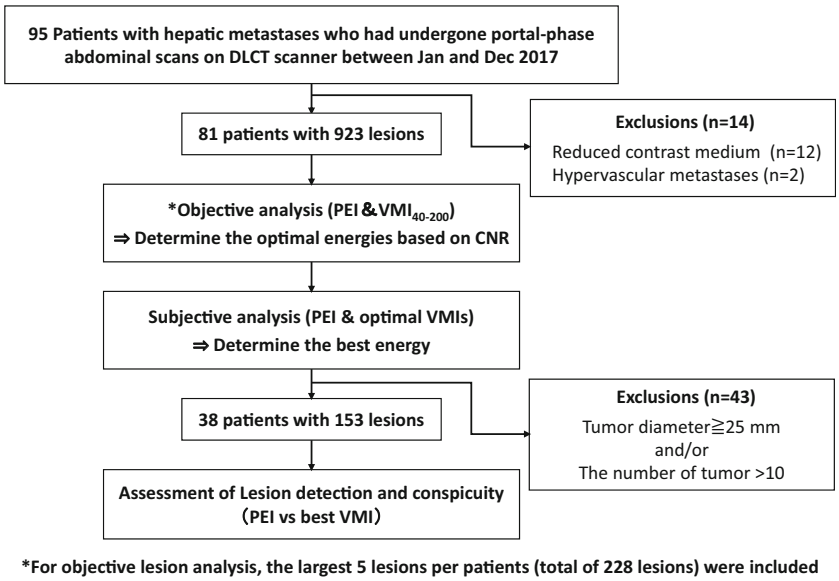

Fig. 1 Study design flowchart with inclusion and exclusion criteria

64 × 0.625; rotation time, 0.5 s. The portal venous phase images were acquired 70 s after the contrast agent (iopamidol, Iopamiron-370; Bayer Healthcare; or iohexol, Omnipaque-300; Daiichi-Sankyo) was delivered at an iodine dose of 600 mgI/kg over 33 s via an antecubital vein. PEI was reconstructed using a hybrid iterative reconstruction algorithm (iDose^4 level 3, Philips Healthcare). VMI was reconstructed at 40–200 keV ($VMI_{40–200}$) with 10-keV intervals using a spectral reconstruction algorithm (Spectral level 3, Philips Healthcare) at a level of noise reduction similar to that of iterative reconstruction used for PEI. All axial images were reconstructed with 2-mm slice thickness.

Radiation dose estimation

The volume CT dose index ($CTDI_{vol}$) was recorded, and the size-specific dose estimates (*SSDE* in the following equation) were calculated on the basis of each patient's effective diameter, as measured on the axial images at the mid-liver level [22]:

$$SSDE = \left(3.70 \times e^{-0.0367 \times \text{effective diameter}}\right) \times CTDI_{vol}$$

Objective analysis

Two board-certified radiologists with 10 and 21 years of experience, respectively, in abdominal CT performed the objective image analysis. The attenuation of liver parenchyma (HU_{liver}) and spinal erector muscle (HU_{muscle}) were measured by placing circular regions of interest (ROIs). The image noise was defined as the standard deviation (SD) of the HU_{muscle}. Each ROI were placed by consensus of the two radiologists, and measurements were performed twice to ensure consistency, with the averaged values being used for the analysis. The contrast-to-noise ratio (CNR) of the liver was calculated as follows:

$$(HU_{liver}\text{-}HU_{muscle})/\text{image noise}$$

For objective lesion analysis, the top five lesions (in terms of maximal diameter) were included when patients had more than five hepatic metastases. Finally, we quantitatively evaluated 288 hepatic metastases (23 ± 18 mm in diameter) in 81 patients. The attenuation of the metastases and surrounding hepatic parenchyma were measured by placing ROIs, and the tumor-to-liver contrast was calculated as the difference between the CT attenuation of the tumor and the hepatic parenchyma. The tumor CNR was calculated by dividing the tumor-to-liver contrast by the image noise.

Subjective analysis

Two board-certified radiologists with 8 and 13 years of experience, respectively, in abdominal CT independently evaluated the subjective quality of PEI and VMI at optimal energies (i.e., VMIs showing significantly higher CNR compared with PEI in objective analysis). The readers were blinded to any patient information and acquisition parameters. The images were randomized and presented using a soft-tissue window with the window adjustment being encouraged for appropriate image interpretation. Five-point scales were used and the scores were as follows: image contrast (1 = undiagnostic; 2 = suboptimal; 3 = average; 4 = good; and 5 = excellent), image noise (1 = undiagnostic; 2 = severe; 3 = moderate; 4 = mild; and 5 = absent), and diagnostic confidence for liver lesion detection (1 = undiagnostic; 2 = suboptimal, low confidence; 3 = average; 4 = above average; and 5 = most confidence). To familiarize the readers with the grading system, a training

session was provided before the evaluations using three cases which were not included in this study. The two readers' average scores were used for the statistical analysis.

Lesion detection

Among the 81 patients, 43 patients, each having more than 10 metastatic nodules and/or metastases ≥ 25 mm in maximum diameter, were excluded from the evaluation of lesion detection performance. Therefore, 38 patients (15 men, 23 women; mean age, 65.4 ± 11.2 years; BMI, 21.6 ± 3.3 cm/kg^2) with 153 lesions (mean diameter, 11 ± 5 mm) were evaluated. Two radiologists with 4 and 7 years of experience in abdominal imaging independently evaluated the PEI and VMI at the best energy defined as the monoenergetic level where the mean tumor CNR and the subjective score for diagnostic confidence were maximized in preceding objective and subjective analysis. Readers understood that each patient might have hepatic metastases, while being blinded to any other information including image reconstruction and the number and location of the metastases. PEI and VMI images were presented in a random order and at least 1 month apart in the same patient to reduce recall bias. Each portal-venous-phase image was presented with a soft-tissue window, with the adjustment of window settings being encouraged to appropriately delineate the hepatic lesions. They were asked to independently identify and mark the possible hypovascular metastases and assign a conspicuity score to each lesion using a following ordinal scale (1 = undetectable, 2 = unclear but detectable, 3 = moderately detectable, 4 = easily detectable, and 5 = most obvious), in which a score of 1 was retrospectively assigned for the lesions not detected by each reader. Matching of reference and reader markings saved as image files was performed following the consensus of two board-certified radiologists with 10 and 21 years of experience, respectively.

Statistical analysis

The continuous variables are expressed as means ± SDs and normal distributions were confirmed with the Kolmogorov–Smirnov test. Paired *t* test was used for comparisons of quantitative valuables between PEI and VMI. The correlation between BMI and image noise or tumor CNR on PEI and VMI at the energy yielding the highest mean CNR was evaluated with Pearson's correlation coefficient. The subjective scores were compared by the Kruskal–Wallis test with Steel's post hoc test serving the scores assigned to PEI as controls. The lesion detection rate and conspicuity scores between PEI and VMI at the best energy were compared with McNemar and Wilcoxon signed-rank test, respectively. To clarify the lesion features benefited by the VMI reconstruction, the lesion size, tumor-to-liver contrast, tumor CNR, and hepatic CNR between the lesions detected only in VMI and lesions detected in both PEI and VMI were compared using Mann–Whitney test. The kappa coefficients for assessing interobserver variabilities on subjective quality and lesion detection and conspicuity were defined as follows: < 0.20 = poor, 0.21–0.40 = fair, 0.41–0.60 = moderate, 0.61–0.80 = substantial, and 0.81–1.00 = excellent. Differences of $p < 0.05$ were considered statistically significant. All analyses were performed with the statistical software R (version 2.6.1; www.r-project.org/).

Results

Radiation dose

$CTDI_{vol}$ and SSDE were 10.5 ± 2.1 mGy and 15.4 ± 1.9 mGy, respectively.

Objective analysis

The image noise of VMI subtly increased as the energy decreased but remained at a low level throughout the energy spectrum (from 12.2 ± 2.4 HU at VMI_{200} to 13.7 ± 2.7 HU at VMI_{40}), which was significantly lower than that observed in PEI (15.1 ± 2.7 HU, $p < 0.01$) (Fig. 2a). Tumor-to-liver contrast and CNR of the hepatic parenchyma and tumors (288 lesions in 81 patients) gradually increased as the monoenergetic level decreased. Compared with PEI, the tumor-to-liver contrast of VMI was significantly higher at 40–60 keV (54.2 ± 17.5 vs. 126.6 ± 56.2–67.4 ± 25.1 HU, $p < 0.001$; Fig. 2b), and CNR of hepatic parenchyma and metastases was significantly higher at 40–70 keV (hepatic CNR: 3.3 ± 0.9 vs. 11.1 ± 3.8–4.1 ± 1.3, $p < 0.001$; tumor CNR: 3.2 ± 1.3 vs. 8.2 ± 3.9–3.9 ± 1.6, $p < 0.001$, Fig. 2c, d). A moderate correlation was found between BMI and image noise for PEI and VMI_{40} (PEI: $r^2 = 0.16$, $p < 0.01$; VMI40: $r^2 = 0.2$, $p < 0.01$) (Fig. 3a, b). No statistically significant correlation was observed between BMI and tumor CNR for VMI_{40} ($r^2 = 0.01$, $p = 0.1$), whereas very weak but significant negative correlation was observed for PEI ($r^2 = 0.03$, $p = 0.005$) (Fig. 3c, d).

Subjective analysis

The image contrast of $VMI_{40–60}$ was rated as superior to that of PEI ($p < 0.01$), whereas no significant difference was observed between VMI_{70} and PEI ($p = 0.3$). $VMI_{40–70}$ was rated as having less noise than PEI ($p < 0.01$). The highest score for diagnostic confidence was assigned for VMI_{40} followed by $VMI_{50–70}$, all of which were better than that of PEI ($p < 0.01$). There was substantial inter-reader agreement (Table 1).

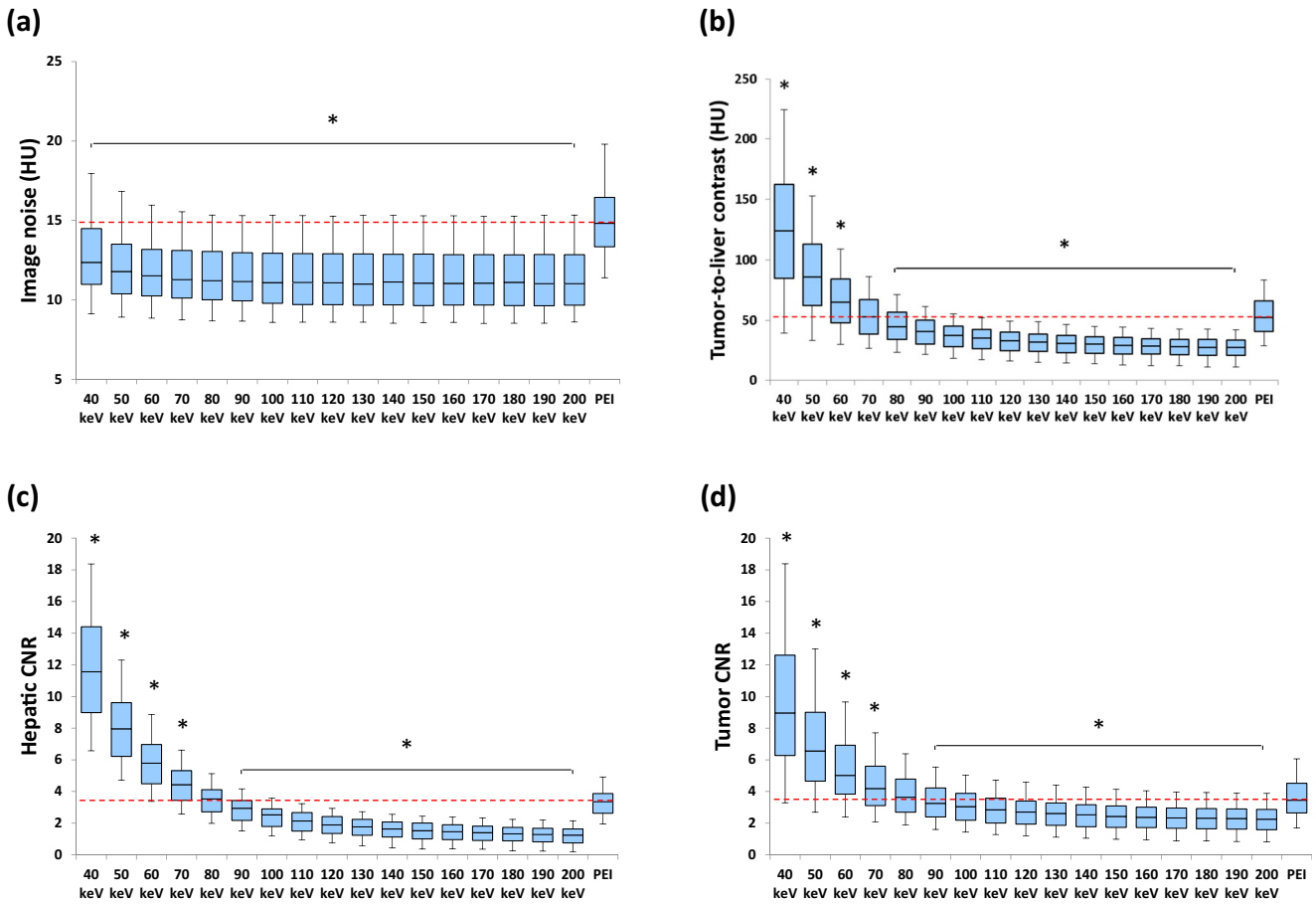

Fig. 2 Box-and-whisker plots of (**a**) image noise, (**b**) tumor-to-liver contrast, (**c**) hepatic CNR, and (**d**) tumor CNR in PEI and VMI at different keV levels. Each box shows the upper and lower quartiles with median value being shown by the horizontal line within each box. Horizontal dotted lines show the median values on PEI. For each energy level, asterisks indicate statistically significant differences, compared with PEI. For the measurement of tumor-to-liver contrast and tumor CNR, the largest five lesions per patients (total 228 lesions in 81 patients) were included

Lesion detection

On the basis of the results of subjective and objective analysis, the lesion detectability and conspicuity were compared between PEI and VMI_{40}. Among the 153 metastases assessed, 77 (50.3%) had diameters of < 10 mm (6.5 ± 1.4 mm) and 76 (49.7%) had diameters of 10–24 mm (14.5 ± 3.8 mm). Table 2 summarizes the results of the lesion detection assessments according to lesion size. The overall detection performance of VMI_{40} was significantly better than PEI ($p < 0.01$). Inter-reader agreement in the overall detection performance for both image sets was excellent ($\kappa = 0.85$ and 0.82 for PEI and VMI_{40}, respectively). Subgroup analysis revealed that VMI_{40} improved detection performance, especially for metastases with small diameters (< 10 mm). Table 3 shows lesion characteristics that would potentially benefit by the use of VMI_{40} during lesion detection. Compared with metastases detected in both PEI and VMI_{40}, metastases detected only in VMI_{40} were significantly smaller in diameter and had lower tumor-to-liver contrast and tumor CNR ($p < 0.001$). The tumor-to-liver contrast and tumor CNR of these lesions increased by 138 and 154%, respectively, from PEI to VMI_{40}.

Conspicuity scores assigned for VMI_{40} were significantly higher than those for PEI, regardless of lesion size ($p < 0.01$) (Table 4). Compared with PEI, 93/153 (60.8%) and 105/153 (68.6%) lesions were assigned better scores on VMI_{40} by readers 1 and 2, respectively. The same score was assigned for 55/153 (35.9%) and 46/153 (30%) lesions by readers 1 and 2, respectively. Five lesions (3.3%) were assigned inferior scores for VMI_{40} by at least one reader. Inter-reader agreement was substantial ($\kappa = 0.61$–0.63 and 0.63–0.69 for PEI and VMI_{40}, respectively). Representative cases are shown in Figs. 4, 5, and 6.

Discussion

In this study, we investigated the impact of VMI derived from DLCT on the image quality and lesion detectability for hypovascular hepatic metastases using conventional PEI as a reference standard. Our results demonstrated that $VMI_{40–70}$ yields a significantly better objective and subjective image quality than PEI. The best diagnostic image quality was

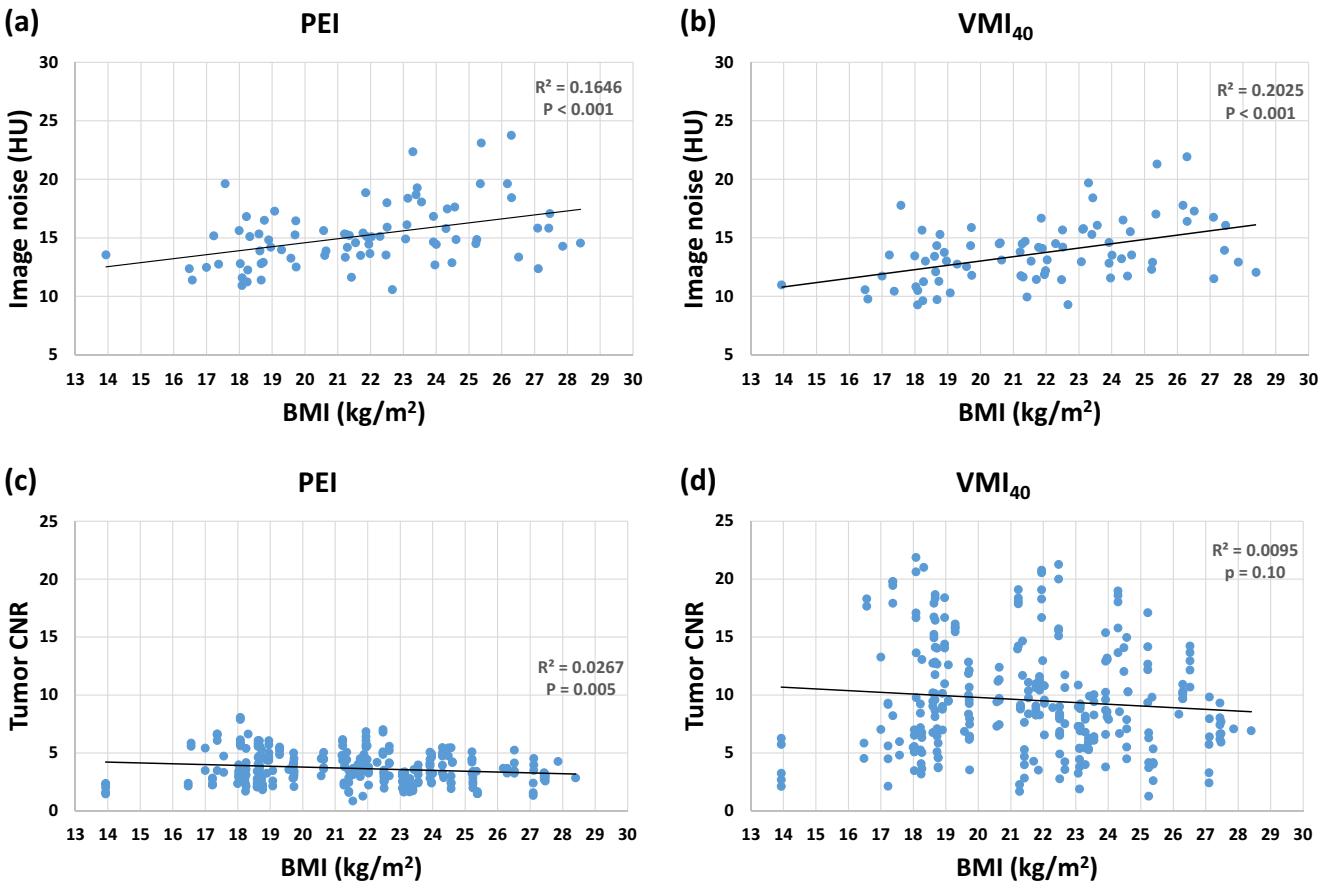

Fig. 3 Associations between BMI and image noise (**a**, **b**) and between BMI and tumor CNR (**c**, **d**) in PEI and VMI_{40}, respectively (Pearson's correlation coefficients)

attained at VMI_{40} owing to the highest iodine contrast without increasing image noise, yielding better lesion detectability, especially for small (< 1 cm) metastatic nodules.

So far, few studies have investigated the added value of VMI for the assessment of hypovascular hepatic metastases during the portal venous phase. Yamada et al and Sudarski et al, who used the tube-based DECT-VMI, revealed that the highest CNR of hypovascular metastases could be attained at around 70 keV and substantially increased noise deteriorated the diagnostic value of lower-keV images [14, 15]. Recently, dual-source DECT addressed the problem of increased noise by introducing an advanced noise-optimized reconstruction algorithm, which provided increased CNR and diagnostic usability with lower-keV VMI for the assessment of hepatic lesions [13, 16, 23]. However, Caruso et al [16] and Husarik et al [23], who evaluated the feasibility of this advanced algorithm for the assessment of hypoattenuating hepatic lesions, have provided mixed results regarding the monoenergetic level for obtaining the best lesion depiction (50 keV in the former and 190 keV in the latter), probably mainly due to differences in study design. Nevertheless, both authors commonly implied that substantial increase in noise restricts the diagnostic usability of VMI at the lowest energy range (i.e., 40 keV). Given the inherent differences in the image characteristics of

Table 1 Subjective analysis

	PEI	VMI_{70}	VMI_{60}	VMI_{50}	VMI_{40}	Kappa
Image contrast	2.8 ± 0.4	2.9 ± 0.4	*3.8 ± 0.4	*4.2 ± 0.4	*4.7 ± 0.4	0.80
Image noise	2.6 ± 0.4	*3.3 ± 0.5	*3.6 ± 0.4	*3.8 ± 0.5	*4.1 ± 0.5	0.68
Diagnostic confidence	2.7 ± 0.4	*3.2 ± 0.5	*3.6 ± 0.5	*4.1 ± 0.4	*4.3 ± 0.5	0.75

Data shown are mean ± standard deviation. The kappa values represent the inter-rater reproducibility in all image sets

PEI polyenergetic image, *VMI* virtual monoenergetic image

*VMI > PEI ($p < 0.01$)

Table 2 Lesion detectability of PEI and VMI_{40} according to lesion size

	All lesions ($n = 153$)			Lesions > 10 mm ($n = 76$)			Lesions < 10 mm ($n = 77$)		
	PEI	VMI_{40}	*p* value	PEI	VMI_{40}	*p* value	PEI	VMI_{40}	*p* value
Reader 1	123/153 (80.0%)	143/153 (93.5%)	< 0.001	72/76 (94.7%)	74/76 (97.4%)	0.48	52/77 (67.5%)	69/77 (89.6%)	< 0.001
Reader 2	116/153 (75.8%)	139/153 (90.1%)	< 0.001	67/76 (88.2%)	73/76 (96.0%)	0.04	49/77 (63.6%)	67/77 (87.0%)	< 0.001
Total	239/306 (78.1%)	282/306 (92.2%)	< 0.001	139/152 (91.4%)	147/152 (96.7%)	0.01	102/146 (69.9%)	136/154 (88.3%)	< 0.001
Kappa	0.85	0.82	NA	0.61	0.66	NA	0.91	0.75	NA

Data are shown in number (%)

NA not applicable, *PEI* polyenergetic image, *VMI_{40}* virtual monoenergetic image at 40 keV

VMI according to different DECT technologies and reconstruction processes [19, 24], we sought the optimal energy levels for DLCT-VMI and its effect on the detection performance, especially for small metastatic nodules.

As expected, the tumor-to-liver contrast gradually increased as the energy decreased with it being equivalent to PEI at 70 keV and 134% higher at 40 keV. The difference in iodine concentrations between hypovascular metastases and hepatic parenchyma at the portal venous phase can be emphasized at lower energies because of the proximity to the iodine K-edge [8]. Additionally, we observed an almost constant quantitative image noise across the entire energy spectrum, which was consistently lower than that in PEI. As a result, VMI_{40} demonstrated a 156% higher tumor CNR than PEI. This may help to improve the lesion delineation and detection performance. The homogeneous noise behavior may be a notable aspect of DLCT, which is especially important for oncological assessments involving low-contrast resolution, such as for the detection of subtle hepatic or pancreatic tumors. Beyond the consistent quantitative image noise, the grainy appearance was less perceptible as the energy decreased

Table 3 Comparison of characteristics between lesions missed in PEI but detected in VMI and detected in both PEI and VMI

	Missed in PEI but detected in VMI_{40}	Detected in both PEI and VMI_{40}	*p* value
Reader 1			
Number of lesions (%)	20/153 (13.1)	123/153 (80.4)	NA
Maximum diameter (mm)	6.9 ± 3.5 (4–20)	11.4 ± 4.9 (4–24)	< 0.01
Tumor-to-liver contrast (HU)			
PEI	21.8 ± 9.8 (7–39)	43.9 ± 16.8 (17–88)	< 0.01
VMI_{40}	51.9 ± 21.5 (19–108)	93.4 ± 48.7 (29–244)	< 0.01
Tumor CNR			
PEI	1.3 ± 0.6 (0.3–2.4)	2.6 ± 1.1 (0.7–6.5)	< 0.01
VMI_{40}	3.3 ± 1.3 (1.6–5.5)	6.3 ± 3.4 (1.0–20.0)	< 0.01
Hepatic CNR			
PEI	2.8 ± 1.0 (1.7–4.6)	2.7 ± 1.0 (0.8–5.4)	0.85
VMI_{40}	10.6 ± 3.7 (6.0–17.1)	9.5 ± 3.3 (2.2–19.3)	0.12
Reader 2			
Number of lesions (%)	24/153 (15.7)	116/153 (75.8)	NA
Maximum diameter (mm)	7.4 ± 3.8 (4–20)	11.5 ± 5.0 (4–24)	< 0.01
Tumor-to-liver contrast (HU)			
PEI	24.6 ± 11.6 (7–46)	44.8 ± 16.7 (17–88)	< 0.01
VMI_{40}	54.6 ± 24.7 (19–108)	101.5 ± 48.2 (29–244)	< 0.01
Tumor CNR			
PEI	1.3 ± 0.6 (0.5–2.2)	2.6 ± 1.1 (0.9–6.5)	< 0.01
VMI_{40}	3.2 ± 1.3 (1.0–5.9)	6.6 ± 3.3 (1.3–20.0)	< 0.01
Hepatic CNR			
PEI	2.4 ± 0.9 (1.0–4.5)	2.7 ± 1.1 (0.9–6.5)	0.36
VMI_{40}	9.2 ± 2.9 (5.1–17.2)	9.7 ± 3.4 (2.3–19.4)	0.44

Data are shown in number (%) or mean ± standard deviation

Table 4 Conspicuity score assigned for each image set according to lesion size

	All lesions ($n = 153$)			Lesion > 10 mm ($n = 76$)			Lesion < 10 mm ($n = 77$)		
	PEI	VMI_{40}	p value	PEI	VMI_{40}	p value	PEI	VMI_{40}	p value
Reader 1	2.5 ± 1.0	3.1 ± 1.1	< 0.01	3.1 ± 0.9	3.8 ± 0.9	< 0.01	1.8 ± 0.7	2.5 ± 0.8	< 0.01
Reader 2	2.2 ± 1.0	3.0 ± 1.2	< 0.01	2.8 ± 1.0	3.7 ± 1.1	< 0.01	1.7 ± 0.6	2.4 ± 0.8	< 0.01
Reader 1 + 2	2.5 ± 1.0	3.1 ± 1.2	< 0.01	3.0 ± 1.0	3.7 ± 1.0	< 0.01	1.8 ± 0.7	2.4 ± 0.8	< 0.01
Kappa	0.63	0.69	NA	0.61	0.67	NA	0.63	0.63	NA

Data are shown in number (%)

NA not applicable, *PEI* polyenergetic image, *VMI_{40}* virtual monoenergetic image at 40 keV

because wider window settings were used in lower energy VMI for appropriate image interpretation [25].

The noise characteristic of DLCT-VMI observed in this study are consistent with recent investigations on DLCT [17, 18, 20], but in contrast to the results of studies on tube-based abdominal DECT [11–16, 23]. Sellerer et al, who directly compared the imaging performance between different DECT platforms, also found that the DLCT provides constant noise levels over the full range of energies, whereas tube-based DECT showed substantial increased noise for lower energy levels [19]. The noise behavior of DLCT-VMI that is distinctly different from tube-based DECT-VMI can be explained by the detector-based DECT solution. In tube-based DECT systems, dual-energy data is postprocessed only in the image domain (dual-source, split-beam, and dual-spin DECT), or angular and temporal interpolation is required before postprocessing in the projection domain (rapid kVp switching DECT). This theoretically leads to deterioration of spatial and temporal resolution, and amplification of the so-called anti-correlated noise, especially at low energies [18]. Contrastingly, the detector-based DECT enables postprocessing in projection domain without angular and temporal interpolation due to perfectly registered dual-energy data. This allows the implementation of anti-correlated noise reduction algorithm, which facilitates the exploitation and cancelation of the anti-correlated noise in the process of VMI reconstruction. Additionally, further noise reduction can be achieved owing to projection-based iterative methods for the spectral image reconstruction [17, 18, 20].

Our results implied that small (approximately 7 mm) and low-contrast (approximately 20–25 HU at PEI) lesions, which were potentially missed on PEI, were detectable by increasing the tumor-to-liver contrast and CNR with use of VMI_{40}. Conversely, relatively large (approximately 11 mm) and high-contrast (approximately 45 HU at PEI) lesions were readily detectable on PEI and thus, improved detection was not achieved with use of VMI_{40}. These observations are in line with the results of experiment by Schindera et al, who demonstrated that the detection of small (6 mm) and low-contrast (20 HU) lesions could be substantially improved as the tumor-to-liver contrast increased, whereas no further improvement was seen for relatively large (10 and 14 mm) and high-contrast (35 HU) lesions [3].

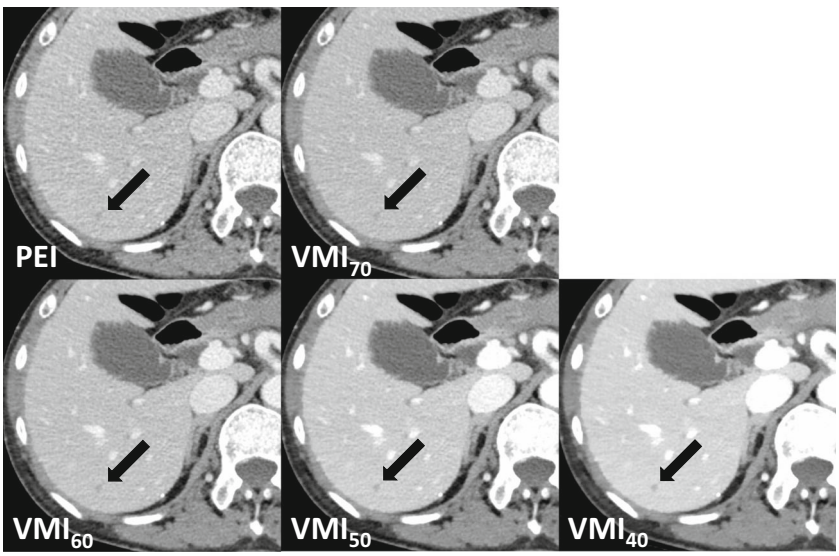

Fig. 4 CT images of a 61-year-old female with hepatic metastases from lung cancer. The conspicuity of a subtle hepatic metastasis (arrows) gradually improves as the energy decreases. This lesion was missed at PEI but correctly detected at VMI_{40} by both readers. Note that the image noise in VMI was less perceptible as the energy decreased because a wider window display was used for lower energy images to achieve appropriate image interpretation

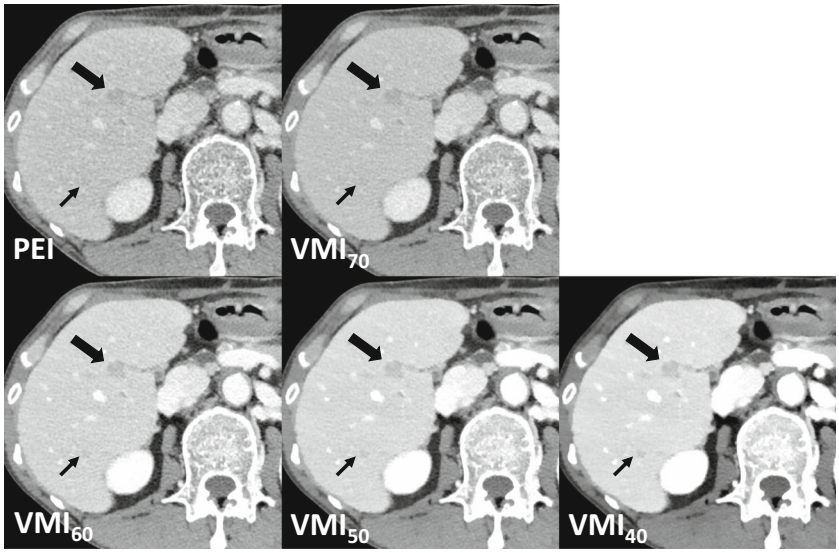

Fig. 5 The CT images from a 65-year-old male with hepatic metastases from esophageal cancer. The small and low-contrast hepatic metastasis (maximum diameter 5 mm, tumor-to-liver contrast at PEI 18 HU, small arrows) were scantly visible at PEI, but became gradually conspicuous on VMI as the energy level decreased. This lesion was correctly identified only at VMI_{40} by both readers. Although a relatively large and high-contrast lesion (maximum diameter 11 mm, tumor-to-liver contrast at PEI 32 HU; large arrows) also became gradually more conspicuous as the energy decreased, this lesion may be confidently detectable, even with PEI

Although VMI_{40} yielded higher conspicuity scores than PEI for most lesions, lower scores were assigned for a few lesions. This observation may be potentially explained by the fact that hypoattenuating nodules containing similar (or more) amounts of iodine relative to hepatic parenchyma theoretically showed no contrast improvement and even become less conspicuous at lower keV, especially when a wider window display was used. A similar phenomenon was reported by Husarik et al, who showed that the iodine-containing hypoattenuating lesions, which were inserted in liver phantoms not containing iodine, become less conspicuous at lower keV [23]. Given that each metastatic nodule can contain various amounts of iodine relative to the hepatic parenchyma, simultaneous review of VMI_{40} and conventional PEI (or

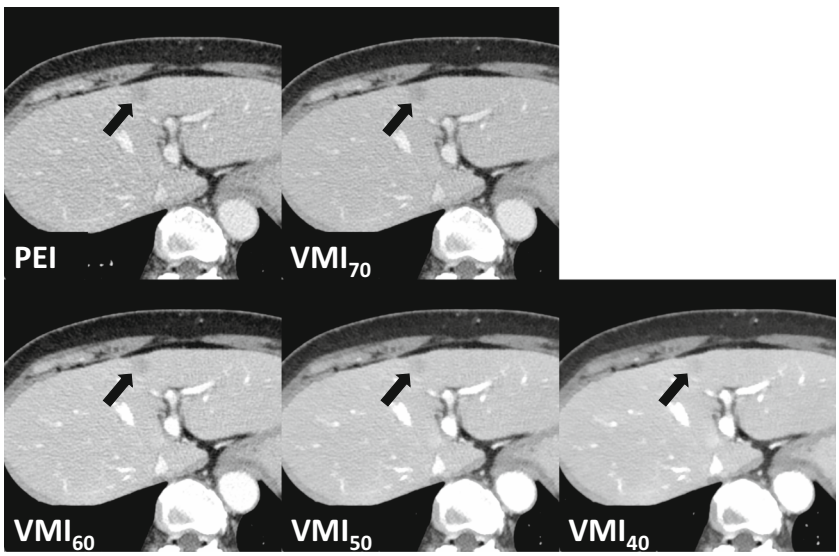

Fig. 6 CT images of a 70-year-old female with a hepatic metastasis (maximum diameter 11 mm, arrows) from breast cancer. Window width and level (W/L) were adjusted for each image (W/L were 350/50, 350/50, 370/60, 450/75, 570/90 HU at PEI, VMI_{70}, VMI_{60}, VMI_{50}, and VMI_{40}, respectively). Compared with PEI, the lesion conspicuity was somewhat degraded at VMI_{40} (conspicuity scores assigned for PEI and VMI_{40} were 3 and 2, respectively, for both readers) despite the higher hepatic attenuation and the lower perceptible noise. Tumor-to-liver contrast were 35, 34, 32, 29, and 24 HU at PEI, VMI_{70}, VMI_{60}, VMI_{50}, and VMI_{40}, respectively. The reasons for the inferior tumor-to-liver contrast at low keV images are unclear, but a possible explanation is that this tumor contained subtly more iodine, relative to the surrounding hepatic parenchyma. In addition, wider window display used for lower keV images may negatively affect the visual conspicuity

VMI at higher energy such as VMI_{70}) may be recommended for accurately detecting any type of lesion without omission.

This study has several limitations. First, the sample size was relatively small, and larger scale studies should be conducted to generalize our results. Second, our patients had smaller body sizes than the Westerners. Previous studies showed that image noise is substantially increased and CNR is decreased at low keV, especially when scanning large objects [11, 23, 26]. Compared with PEI, we observed no substantial increase in noise or decrease in CNR at VMI_{40} in patients with relatively large BMIs. Nevertheless, whether our results can apply to wider populations should be determined by future studies. Third, we could not compare the diagnostic accuracy owing to the lack of histologic proof or imaging reference standards, as was the case with some previous studies [8–10, 27]; instead, we focused on assessing the subjective and objective image quality and lesion detection performance. The portal-venous-phase CT images have generally limited value for differentiating small hypoenhancing hepatic lesions [28]; therefore, clarifying whether the DLCT-derived iodine overlay map or spectral curve analysis can improve the diagnostic accuracy for differentiating these lesions could be an important research subject in the future [29, 30]. Finally, because we evaluated patients with histories of hepatic metastases known by the readers, the detection performance may have been overestimated and cannot be immediately extrapolated to the general oncology population.

In conclusion, $VMI_{40–70}$ yields a better image quality for the assessment of hypovascular hepatic metastases than conventional PEI. The best objective and subjective image quality was attained at VMI_{40}, wherein we noted superior detectability and conspicuity for most lesions, especially for the metastatic nodules with a diameter of < 1 cm. Given that a few metastatic nodules can become less conspicuous at lower keV, the combined review of VMI_{40} and conventional PEI (or VMI at higher energy such as VMI_{70}) may be recommended for accurately detecting any type of lesions.

Funding The authors state that this work has not received any funding.

Compliance with ethical standards

Guarantor The scientific guarantor of this publication is Yasuyuki Yamashita.

Conflict of interest The authors of this manuscript declare no relationships with any companies, whose products or services may be related to the subject matter of the article.

Statistics and biometry No complex statistical methods were necessary for this paper.

Ethical approval Institutional Review Board approval was obtained.

Informed consent Written informed consent was waived by the Institutional Review Board.

Methodology
- Retrospective
- Observational
- Performed at one institution

References

1. Ward J, Robinson PJ, Guthrie JA et al (2005) Liver metastases in candidates for hepatic resection: comparison of helical CT and gadolinium- and SPIO-enhanced MR imaging. Radiology 237: 170–180
2. Niekel MC, Bipat S, Stoker J (2010) Diagnostic imaging of colorectal liver metastases with CT, MR imaging, FDG PET, and/or FDG PET/CT: a meta-analysis of prospective studies including patients who have not previously undergone treatment. Radiology 257:674–684
3. Schindera ST, Hareter LF, Raible S et al (2012) Effect of tumor size and tumor-to-liver contrast of hypovascular liver tumors on the diagnostic performance of hepatic CT imaging. Invest Radiol 47: 197–201
4. Judy PF, Swensson RG, Szulc M (1981) Lesion detection and signal-to-noise ratio in CT images. Med Phys 8:13–23
5. Kanal KM, Chung JH, Wang J et al (2011) Image noise and liver lesion detection with MDCT: a phantom study. AJR Am J Roentgenol 197:437–441
6. Yamashita Y, Komohara Y, Takahashi M et al (2000) Abdominal helical CT: evaluation of optimal doses of intravenous contrast material–a prospective randomized study. Radiology 216:718–723
7. Awai K, Kanematsu M, Kim T et al (2016) The optimal body size index with which to determine iodine dose for hepatic dynamic CT: a prospective multicenter study. Radiology 278:773–781
8. Robinson E, Babb J, Chandarana H, Macari M (2010) Dual source dual energy MDCT: comparison of 80 kVp and weighted average 120 kVp data for conspicuity of hypo-vascular liver metastases. Invest Radiol 45:413–418
9. Volders D, Bols A, Haspeslagh M, Coenegrachts K (2013) Model-based iterative reconstruction and adaptive statistical iterative reconstruction techniques in abdominal CT: comparison of image quality in the detection of colorectal liver metastases. Radiology 269:469–474
10. Chang W, Lee JM, Lee K et al (2013) Assessment of a model-based, iterative reconstruction algorithm (MBIR) regarding image quality and dose reduction in liver computed tomography. Invest Radiol 48:598–606
11. Marin D, Ramirez-Giraldo JC, Gupta S et al (2016) Effect of a noise-optimized second-generation monoenergetic algorithm on image noise and conspicuity of hypervascular liver tumors: an in vitro and in vivo study. AJR Am J Roentgenol 206:1222–1232
12. Shuman WP, Green DE, Busey JM et al (2014) Dual-energy liver CT: effect of monochromatic imaging on lesion detection, conspicuity, and contrast-to-noise ratio of hypervascular lesions on late arterial phase. AJR Am J Roentgenol 203:601–606
13. De Cecco CN, Caruso D, Schoepf UJ et al (2018) A noise-optimized virtual monoenergetic reconstruction algorithm improves the diagnostic accuracy of late hepatic arterial phase dual-energy CT for the detection of hypervascular liver lesions. Eur Radiol. https://doi.org/10.1007/s00330-018-5313-6
14. Yamada Y, Jinzaki M, Tanami Y, Abe T, Kuribayashi S (2012) Virtual monochromatic spectral imaging for the evaluation of hypovascular hepatic metastases: the optimal monochromatic level with fast kilovoltage switching dual-energy computed tomography. Invest Radiol 47:292–298
15. Sudarski S, Apfaltrer P, Nance JW Jr et al (2014) Objective and subjective image quality of liver parenchyma and hepatic

metastases with virtual monoenergetic dual-source dual-energy CT reconstructions: an analysis in patients with gastrointestinal stromal tumor. Acad Radiol 21:514–522
16. Caruso D, De Cecco CN, Schoepf UJ et al (2017) Can dual-energy computed tomography improve visualization of hypoenhancing liver lesions in portal venous phase? Assessment of advanced image-based virtual monoenergetic images. Clin Imaging 41:118–124
17. Nagayama Y, Nakaura T, Oda S et al (2017) Dual-layer DECT for multiphasic hepatic CT with 50 percent iodine load: a matched-pair comparison with a 120 kVp protocol. Eur Radiol. https://doi.org/10.1007/s00330-017-5114-3
18. Kalisz K, Rassouli N, Dhanantwari A, Jordan D, Rajiah P (2018) Noise characteristics of virtual monoenergetic images from a novel detector-based spectral CT scanner. Eur J Radiol 98:118–125
19. Sellerer T, Noël PB, Patino M et al (2018) Dual-energy CT: a phantom comparison of different platforms for abdominal imaging. Eur Radiol. https://doi.org/10.1007/s00330-017-5238-5
20. Große Hokamp N, Höink AJ, Doerner J et al (2017) Assessment of arterially hyper-enhancing liver lesions using virtual monoenergetic images from spectral detector CT: phantom and patient experience. Abdom Radiol (NY). https://doi.org/10.1007/s00261-017-1411-1
21. Lee SM, Kim SH, Ahn SJ, Kang HJ, Kang JH, Han JK (2018) Virtual monoenergetic dual-layer, dual-energy CT enterography: optimization of keV settings and its added value for Crohn's disease. Eur Radiol 28:2525–2534
22. Christner JA, Braun NN, Jacobsen MC, Carter RE, Kofler JM, McCollough CH (2012) Size-specific dose estimates for adult patients at CT of the torso. Radiology 265:841–847
23. Husarik DB, Gordic S, Desbiolles L et al (2015) Advanced virtual monoenergetic computed tomography of hyperattenuating and hypoattenuating liver lesions: ex-vivo and patient experience in various body sizes. Invest Radiol 50:695–702
24. Jacobsen MC, Schellingerhout D, Wood CA et al (2018) Intermanufacturer comparison of dual-energy CT iodine quantification and monochromatic attenuation: a phantom study. Radiology 287:224–234
25. Doerner J, Wybranski C, Byrtus J et al (2017) Intra-individual comparison between abdominal virtual mono-energetic spectral and conventional images using a novel spectral detector CT. PLoS One 12:e0183759
26. Leng S, Yu L, Fletcher JG, McCollough CH (2015) Maximizing iodine contrast-to-noise ratios in abdominal CT imaging through use of energy domain noise reduction and virtual monoenergetic dual-energy CT. Radiology 276:562–570
27. Shuman WP, Chan KT, Busey JM et al (2014) Standard and reduced radiation dose liver CT images: adaptive statistical iterative reconstruction versus model-based iterative reconstruction-comparison of findings and image quality. Radiology 273:793–800
28. Onishi H, Murakami T, Kim T et al (2006) Hepatic metastases: detection with multi-detector row CT, SPIO-enhanced MR imaging, and both techniques combined. Radiology 239:131–138
29. De Cecco CN, Darnell A, Rengo M et al (2012) Dual-energy CT: oncologic applications. Am J Roentgenol 199:S98–S105
30. Wang Q, Shi G, Qi X, Fan X, Wang L (2014) Quantitative analysis of the dual-energy CT virtual spectral curve for focal liver lesions characterization. Eur J Radiol 83:1759–1764